Building and Environment 96 (2016) 131–141

Contents lists available at ScienceDirect

Building and Environment

journal homepage: www.elsevier.com/locate/buildenv

Prompt design of the air-supply opening size for a commercial airplane based on the proper orthogonal decomposition of flows

Yun Wei, Tengfei (Tim) Zhang*, Shugang Wang

School of Civil Engineering, Dalian University of Technology (DUT), 2 Linggong Road, Dalian 116024, China

ARTICLE INFO

Article history:
Received 12 August 2015
Received in revised form
1 November 2015
Accepted 20 November 2015
Available online 2 December 2015

Keywords:
Prompt design
POD
Data samples
Interpolation
CFD
Aircraft cabin

ABSTRACT

Air supply is crucial for creating an acceptable air distribution inside aircraft cabins. To determine proper air-supply parameters, a conventional design has to solve many cases to obtain the flow patterns for each air-supply parameter, which is time-consuming. This study proposed a proper orthogonal decomposition (POD) of the flows to accelerate the design. A few original thermo-flow data samples are obtained using a full CFD simulation, and then the orthogonal spatial modes and their coefficients are extracted from these data samples. A trial and data sample increase scheme is used to determine whether the CFD-provided data samples are sufficient. A shape-preserving interpolation is applied to estimate the coefficients of the spatial modes between two neighboring data samples. With a quick map of the thermo-flow fields, the proper air-supply parameters can be rapidly determined based on the specific design criteria. The proposed method was applied to determine the size of an air-supply opening in a three-dimensional aircraft cabin, with the percentage of dissatisfied (PD), the predicted mean vote (PMV) and the mean age of air as the design criteria. The results show that the POD-based design is able to construct the field data with generally good accuracy. The inversely determined air-supply opening sizes between the proposed method and the full CFD simulation are quite similar. Future research may explore a better coordination between the original data sample preparation using the full CFD simulation and the interpolation of the coefficients of the spatial modes to further reduce the computing time.

1. Introduction

Proper air distribution is crucial for maintaining a comfortable thermal environment and good air quality in enclosed spaces. To design an appropriate air distribution, a cause-effect relationship must be established between the air-supply parameters and the resulting environmental performance. This cause-effect relationship is governed by the Navier–Stokes (N–S) equations. Because of the nonlinearity in the N–S equations, mapping the cause-effect from a design parameter to the interior environmental performance is not straightforward. It is challenging to determine the exact air-supply parameters that can create the target performance of thermal comfort and interior air quality. The current design would require a lengthy iterative trial-and-error procedure, by enumerating every possible air-supply parameter to find an optimal solution. An inverse design is able to provide a faster approach for fulfilling the task by setting the design targets first and then inversely solving for the required causal boundary parameters. This approach forms the framework of inverse modeling, i.e., determining causal information from certain expected consequences.

Current inverse modeling in indoor environments is primarily constrained to pollutant source identification, such as the determination of pollutant source locations [1–5], quantifying temporal pollutant release rates [6], and judging pollutant release times [7]. These methods may not be applicable to the inverse design of enclosed environments [8]. When identifying pollutant sources in a fixed flow context, an inversion of the passive scalar transport equation is sufficient. However, the inverse design of enclosed environments would require an inversion of the thermo-flow equations, which include a velocity vector, pressure scalar, and temperature scalar; occasionally, all of the above variables are coupled together.

There are only a few studies addressing the inverse design of enclosed environments. Xue et al. [9] developed a CFD-based genetic algorithm to optimize and predict flows in confined spaces. Zhai et al. [10] imposed constraints on a multi-objective genetic

* Corresponding author.
E-mail address: tzhang@dlut.edu.cn (T. Zhang).

http://dx.doi.org/10.1016/j.buildenv.2015.11.020
0360-1323/

Nomenclature

a	coefficient vector of dummy variables or eigenvector
a	element of the coefficient vector **a**
c	coefficient of the POD mode
E	error between the interpolated fields and the CFD simulated fields
f	dummy vector for the velocity, temperature, etc., at all grid points that constitute a vector
f	dummy variable for the velocity, temperature, etc., at a grid point
n	number of eigenvalues for which the general energy exceeds 99.99%
N	number of grid points
P	number of data samples
s	averaged autocorrelation matrix of the fields
s	elements in the averaged autocorrelation matrix
x,**x**′	position vector

Greek variable

φ	orthogonal basis or spatial mode or POD mode
λ	Lagrangian multiplier or eigenvalue of **s**
Ω	domain over which **f**(**x**) is defined

Superscript

i, j	index of a data sample
k	index of a spatial mode

Subscript

i, j	index of an eigenvector
k	index of coefficient of a POD mode
m	index of a grid point

algorithm to design ventilation systems for an aircraft cabin. Zhang and You [11] applied a neural network to optimize air-supply speed and temperature for a commercial aircraft cabin. Currently, no study has inversely determined the sizes of air-supply openings for an enclosed space. In addition, the computing efficiency for both the CFD-based genetic algorithm and the neural network is quite low due to the large number of forward CFD simulations involved.

To accelerate the forward thermo-flow solution, a POD technique was developed. The POD method was proposed by Lumley [12] nearly a half century ago to analyze inhomogeneous turbulent flows. The POD technique provides a basis for the modal decomposition of an ensemble of data, such as the thermo-flow fields obtained from numerical simulations or experiments. The coherent structures of these data that contain the basic features of the fields are extracted. The most important benefit of the POD analysis is its efficiency in capturing the dominant features with only a few modes [13]. Early applications of the POD method consisted of a few near-wall and jet-induced mixing flows [14–16]. Later, the snapshot method [17] was proposed to minimize the dimensions of the POD eigenvalue system. Snapshots are the data samples used for extracting the POD modes, which reduce the dimensions of the eigenvalue system from the number of grid points to the number of snapshots. Generally, the number of snapshots is far less than the number of spatial grid points, and thus a significant amount of computing costs can be saved.

In enclosed environments, the POD is primarily used for the rapid prediction of indoor thermo-flow and pollutant concentrations, optimization of air-supply parameters, and development of controllers for dynamic ventilation control. Elhadidi and Khalifa [18] applied a POD analysis to efficiently predict the indoor velocity and temperature distributions inside an empty office. Ding et al. [19] proposed a POD-based data interpolation to predict the thermo-flow fields for natural and forced convection flows. Sempey et al. [20] performed a POD-based prediction of the temperature distribution in air-conditioned rooms in a fixed-flow context. Allery et al. [21] tracked the particle motion in a two-dimensional ventilated cavity with airflow provided by a POD construction. Li et al. [22] integrated a genetic algorithm into the POD prediction of thermo-flow to efficiently optimize the air-supply velocity and temperature. Ahuja et al. [23] developed POD-based controllers to eliminate the heat disturbance in an indoor environment. Tallet et al. [24] used a POD analysis to dynamically control the window opening for optimizing the indoor environment comfort and quality. Li et al. [25] proposed a POD-based temperature prediction model for the dynamic control of room temperature.

The above review reveals that the current inverse design suffers from a high computing cost. The POD has provided a quick method for obtaining the thermo-flow fields based on a limited number of full CFD simulations. It is viable to use the POD analysis to accelerate the inverse design. This study demonstrates how a POD based model was utilized to promptly determine the size of an air-supply opening in an aircraft cabin. The solution accuracy and the computing costs were compared between the full CFD simulation and our proposed POD approach.

2. Methodologies

In this section, the basic principles of the POD are first outlined, followed by criteria for determining whether the original data samples provided by the full CFD simulation are sufficient. Then the solution procedure for the POD-based prompt design is presented.

2.1. Basic principles of POD analysis

The POD method originates from the decomposition of turbulent flow fields. However, the method can be applied to decompose any data ensemble based on the statistical theory. This investigation has applied the POD to analyze the field data of air velocity, temperature and mean age of air when the air-supply opening sizes are varied. Then a quick map from the air-supply opening size to the velocity, temperature and mean age of air is established. Let **f** represent a dummy vector for velocity, temperature and mean age of air at all grid points that constitute a vector. Suppose that we have an ensemble $\{\mathbf{f}^i\}$, each as a function of the spatial coordinates, i.e., $\mathbf{f} = \mathbf{f}(\mathbf{x})$, where **x** represents a position vector. We can define an orthogonal basis (or spatial mode, or POD mode) φ that captures more information on a variable than any other mode, which is maximized with the projection of **f** onto φ [13] as follows:

$$\max \frac{\left\langle |(\mathbf{f}, \boldsymbol{\varphi})|^2 \right\rangle}{\|\boldsymbol{\varphi}\|^2}, \tag{1}$$

where $(\,,\,)$ represents the inner product, $|\cdot|$denotes the modulus, $\langle\cdot\rangle$ is an averaging operation, and $\|\cdot\|$ is the L^2-norm. Eq. (1) can be recast into the following Euler–Lagrange integral equation [26] as:

$$\int_{\Omega} \langle \mathbf{f}(\mathbf{x})\mathbf{f}^*(\mathbf{x}')\rangle \boldsymbol{\varphi}(\mathbf{x}')d\mathbf{x}' = \lambda\boldsymbol{\varphi}(\mathbf{x}), \tag{2}$$

where * denotes the complex conjugation, λ is a Lagrangian multiplier, and Ω is the domain over which **f**(**x**) is defined. Writing

the ensemble average as an average of the data samples, Eq. (2) can be expressed into:

$$\frac{1}{P}\sum_{j=1}^{P}\mathbf{f}^{j}(\mathbf{x})\int_{\Omega}\mathbf{f}^{j*}(\mathbf{x}')\boldsymbol{\varphi}(\mathbf{x}')d\mathbf{x}'=\lambda\boldsymbol{\varphi}(\mathbf{x}), \tag{3}$$

where P is the number of data samples, superscript j represent the j^{th} data sample. Eq. (3) forms an $N\times N$ eigenvalue system, where N is the number of grid points in the numerical solution. To save computing costs, the snapshot method [17] can be applied to reduce the dimensions of the system into $P\times P$, and typically P is significantly less than N. We can define $a_j=\frac{1}{\lambda P}\int_{\Omega}\mathbf{f}^{j*}(\mathbf{x}')\boldsymbol{\varphi}(\mathbf{x}')d\mathbf{x}'$, and then Eq. (3) can be simplified as follows:

$$\sum_{j=1}^{P}\mathbf{f}^{j}(\mathbf{x})a_j=\boldsymbol{\varphi}(\mathbf{x}). \tag{4}$$

Multiplying $\mathbf{f}^{i*}(\mathbf{x})$ against both sides, integrating over $\mathbf{x}$, Eq. (4) can be rewritten into:

$$\frac{1}{P}\sum_{j=1}^{P}\int_{\Omega}\mathbf{f}^{i*}(\mathbf{x})\mathbf{f}^{j}(\mathbf{x})d\mathbf{x}a_j=\lambda a_i. \tag{5}$$

If we define tensor $s_{ij}=\frac{1}{P}\int_{\Omega}\mathbf{f}^{i*}(\mathbf{x})\mathbf{f}^{j}(\mathbf{x})d\mathbf{x}$ and both i and $j=1,\cdots,P$, then Eq. (5) becomes:

$$\begin{bmatrix}s_{11}&\cdots&s_{1P}\\ \cdots&\ddots&\vdots\\ s_{P1}&\cdots&s_{PP}\end{bmatrix}\begin{bmatrix}a_1\\ \vdots\\ a_P\end{bmatrix}=\lambda\begin{bmatrix}a_1\\ \vdots\\ a_P\end{bmatrix}\quad\text{or}\quad\mathbf{s}\cdot\mathbf{a}=\lambda\mathbf{a}. \tag{6}$$

A more detailed derivation of the POD modes can be found in the textbook [26]. Now Eq. (6) becomes an eigenvalue system of $P\times P$, where vector $\mathbf{a}$ can be treated as an eigenvector, and λ is the corresponding eigenvalue. The eigenvalue represents the energy captured by the POD mode. The general energy is defined as the sum of all of the eigenvalues. Commonly 95% of the general energy is enough for most applications, and such a criterion can be adjusted depending on different purposes and the desired accuracy [18]. In this investigation, 99.99% was selected for determining how many eigenvalues should be used, and we assume this number as n. Once the eigenvector $\mathbf{a}$ and the eigenvalue λ are obtained, the POD mode $\boldsymbol{\varphi}$ can be calculated from Eq. (4).

Then a new data field can be reconstructed as a linear combination of a series of $\boldsymbol{\varphi}$s as:

$$\mathbf{f}_{\text{R}}=\sum_{k=1}^{n}c_k\boldsymbol{\varphi}^{k}, \tag{7}$$

where $\mathbf{f}_{\text{R}}$ is the reconstructed field and c_k is the coefficient of the k^{th} POD mode $\boldsymbol{\varphi}^{k}$. Furthermore, c_k can be calculated by:

$$c_k=\left(\mathbf{f},\boldsymbol{\varphi}^{k}\right). \tag{8}$$

Thus far, Eq. (7) can be applied to reconstruct the sample field $\mathbf{f}_{\text{R}}$ once the coefficients of all of the POD modes are known.

2.2. Original data preparation and criteria for adequate data samples

A few original data samples must be provided by the full CFD simulation to extract the POD modes. Because the cost of a full CFD simulation is extremely high, an efficient design shall keep a minimum load of the full CFD simulation but still be able to ensure accuracy. To determine the appropriate number of data samples from the full CFD simulation, a trial and data sample increase method was proposed. For illustration, Fig. 1 shows example dummy errors between the linearly interpolated sample point and the full CFD simulation sample point versus an air-supply parameter. The linear interpolation of the data points was used for evaluation of the linearity of the provided data samples. Most models including the POD analysis perform poorly when the nonlinearity prevails. The method begins with two original data sample points provided by full CFD simulations, which correspond to the smallest and largest air-supply parameters in the constrained range, as shown by S1 and S2 in Fig. 1. The errors of these two points are zero in Fig. 1, assuming that there is no error from the full CFD simulation. The data sample in the middle of S1 and S2 is estimated by applying a linear interpolation of the field data, as shown by S3 in Fig. 1. Furthermore, a full CFD simulation for the air-supply parameter of S3 should be conducted, as shown by S3′. Then the error between the linearly interpolated field and the full CFD simulation field can be evaluated, whose error is the distance between points S3 and S3′ in Fig. 1. The black dotted curves in Fig. 1 are the errors between the fields provided by the full CFD simulation and the linearly interpolated fields. The error evaluation equations are defined as [22]:

$$E_{\text{average}}=\frac{\sqrt{\left(\sum_{m=1}^{N}\left(f_{\text{interpolated},m}-f_{\text{CFD},m}\right)^{2}\Big/N\right)}}{f_{\text{CFD,normalized}}} \tag{9}$$

and

$$E_{\max}=\frac{\max\left(f_{\text{interpolated},m}-f_{\text{CFD},m}\right)}{f_{\text{CFD,normalized}}},\ m=1,\ \ldots,\ N, \tag{10}$$

where E_{average} represents the average relative error of the interpolated fields, $E_{\max}$ is the maximum relative error, $f_{\text{interpolated}}$ is the interpolated field data, f_{CFD} is the field data by the full CFD simulation, subscript m represents the m^{th} grid cell, and $f_{\text{CFD,normalized}}$ represents the specific value to normalize the relative error. If the relative errors are greater than the set threshold values (such as the blue dashed-dotted line in Fig. 1), the current available data samples (S1 and S2) are not sufficient. Then the new data sample from the full CFD simulation (S3′) is supplemented into the original data samples, and the relative error of S3′ is zero in Fig. 1. Following a similar procedure, the method gradually increases the data samples (S4′ and S5′) until all of the errors between the linearly interpolated data fields and the data fields from the full CFD simulation in the middle of the two neighboring samples are less than the set threshold value, as shown by S6, S7, S8, and S9 in Fig. 1. In this way, the nonlinearity among data samples is weakened, which improves the accuracy of POD mode extraction and the later-on data interpolation.

2.3. Prompt design procedure

Fig. 2 illustrates the POD-based design procedure. The design criteria should be first set, and the two thermo-flow data samples corresponding to the smallest and largest air-supply parameters are solved using full CFD simulations. Then the field data for the middle air-supply parameter are linearly interpolated, and the errors against the full CFD simulations are evaluated. Once there are sufficient original data samples from the CFD, the POD analysis can be conducted to extract the spatial modes and their coefficients. To construct the field data that are not in the original data samples from the CFD, this investigation adopted the piecewise cubic

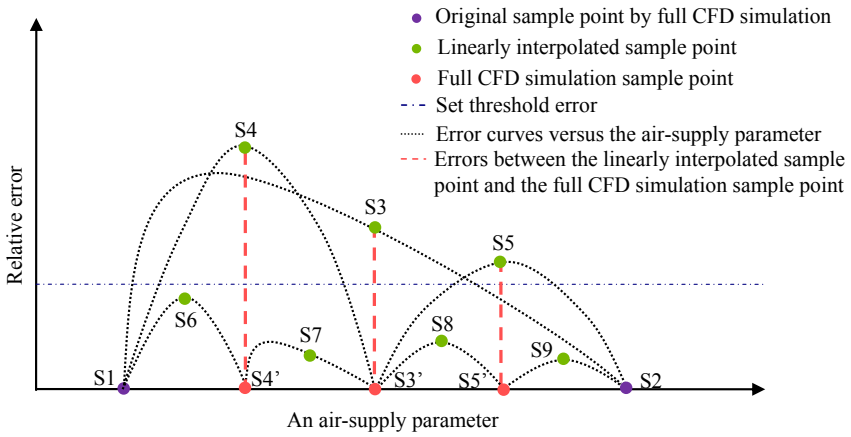

Fig. 1. Illustration of error versus an air-supply parameter to determine whether the CFD provided data samples are adequate.

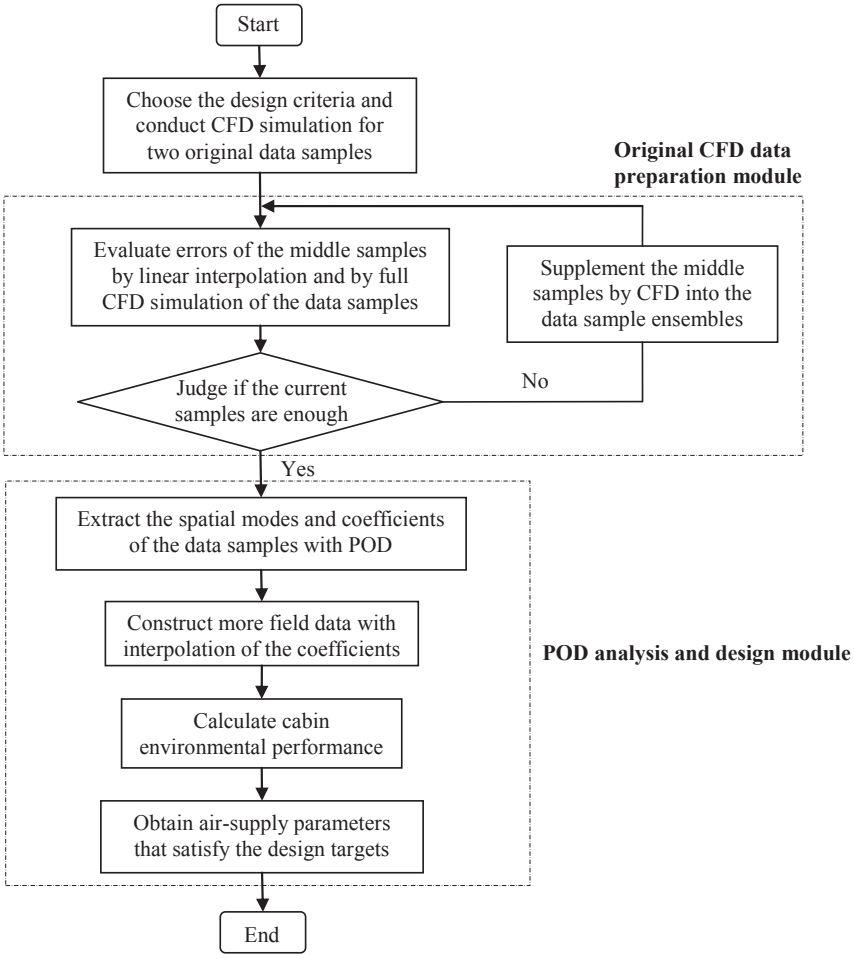

Fig. 2. Solution flow chart for the POD-based design approach.

Hermite interpolation (a shape-preserving interpolation) for the coefficients of the POD modes. The shape-preserving interpolation can preserve the monotonicity and the shape of the data, which ensures that the interpolated curves are smooth. Then the environmental performance can be quickly solved based on the constructed field data, and the air-supply parameters that satisfy the set specific design targets are obtained.

3. A demonstration case

The POD-based design was applied to determine the size of an air-supply opening in a half section of a three-dimensional aircraft cabin, as depicted in Fig. 3(a). There are three passengers seated inside the cabin, which are simulated by simplified thermal manikins. Table 1 summarizes some major thermo-flow boundary conditions, which are consistent with those used in the published

literature [27]. The front and rear boundaries are set as the periodic type and the vertical surface in the aisle is symmetrical. All of the seats are assumed to be adiabatic. Conditioned air is supplied into the cabin horizontally by a linear slot opening on the side wall near the ceiling. The normal direction of the air-supply opening is inclined downwards with an angle of 36.1° from the horizontal. The internal air is exhausted on the side wall near the floor. The air-supply opening size can be varied from 0.5 cm to 4.5 cm. Consequently, the air-supply speeds are varied for the different air-supply opening sizes used.

Fig. 3(b) illustrates the two regions where the performance of the thermal comfort and the air quality is evaluated for the air-supply opening size design. One is the occupied zone highlighted by a blue box in Fig. 3(b), and the other is the breathing zone highlighted by a red box. In the occupied zone, the thermal comfort is evaluated in terms of the percentage of dissatisfied (PD) and the predicted mean vote (PMV). The cabin air quality performance is evaluated using the mean age of air in the breathing zone. The specific design targets state that the largest percentage of dissatisfied (PD) in the occupied zone should be less than 25%, the volumetric-averaged absolute value of the predicted mean vote (PMV) in the occupied zone should be less than 0.56, and the largest mean age of air should be less than 130 s in the breathing zone.

The PD is calculated based on the recommendations provided by the ASHRAE Handbook [28], and the PMV is based on the formula by Fanger [29]. Some parameters involved in the PMV calculation are addressed in the following. The metabolic rate for an adult is 75 W/m^2, and there is no mechanical work production. The water vapor pressure is equal to 475 Pa, which corresponds to a relative humidity of 15% at 25 °C. The clothing area factor is 1.16 and the clothing insulation is assumed to be 1.1 clo, i.e., 0.17 (m·°C)/W. The background mean radiation temperature for the clothed body is 22 °C. The convective heat transfer coefficient and the mean temperature of the outer surface of the clothed body are estimated based on the ASHRAE Handbook [28]. The mean age of air can be easily computed as a passive scalar variable [30] by CFD. Because the PD and the PMV are explicit functions of the velocity and temperature distribution, once the velocity and temperature fields are known, the PD and PMV distribution can be calculated instantly. However, the mean age of air is an implicit function of the velocity field, which can still be quickly solved using the POD analysis.

To resolve the thermo-flow fields using the CFD, the cabin geometry as shown in Fig. 3(a) was created using the GAMBIT software. All air-supply openings were pre-created and the boundary types of the openings can be switched between the air-supply inlet and the solid wall subject to their usage. Hence, the same

Table 1
Boundary conditions for the aircraft cabin.

Item	Value	Item	Value
Passenger surface temperature	30.3 °C	Air-supply flow rate	0.03 m^3/s
Floor temperature	23 °C	Air-supply temperature	19.5 °C
Side wall temperature	22 °C	Lamp temperature	24.7 °C
Ceiling temperature	22 °C		

tetrahedral grids were created in the domain for all cases, and the total grid cell number is 1,279,328. Near the solid walls, human body surfaces, air supply and air exhaust, the grids were further refined to satisfy grid independence. The numerical solutions to the N–S equations were carried out in the FLUENT software (version 6.3.26). The turbulent combined convection flows were resolved using the standard k-ε model along with the enhanced wall treatment. To fully consider thermal buoyancy, the Boussinesq approximation was adopted to represent the varying density with temperature in the momentum equations. In addition, the pressure staggering option (PRESTO) scheme was selected when discretizing the pressure term, whereas the remaining terms were discretized using the second-order upwind scheme. The semi-implicit pressure linked equation (SIMPLE) scheme was used for the pressure and velocity coupling. The convergence was deemed to be satisfactory if the unbalanced heat transfer rate for all of the boundaries was less than 0.5% of the maximum heat gain, and there was no significant change in the temperature, velocity, and mean age of air with numerical iterations at a few typical monitoring points.

When evaluating relative errors using Eqs. (9) and (10), $f_{CFD,normalized}$ was set as the volumetric average speed in the occupied zone for velocity. For example, for the air-supply opening size of 0.5 cm $f_{CFD,normalized}$ = 0.32 m/s and for 4.5 cm $f_{CFD,normalized}$ = 0.13 m/s. For temperature, $f_{CFD,normalized}$ is the temperature difference between the occupant surface (30.3 °C) and the surrounding air (23.5 °C), i.e., 6.8 °C. $f_{CFD,normalized}$ is approximately 101 s for the mean age of air, which is the time constant of the cabin air ventilation. When determining whether a certain number of original data samples are enough, the set threshold of the average relative errors is 10%, while the maximum relative errors are also plotted for reference.

4. Results

4.1. Preparation of original data samples

Based on the solution flow chart in Fig. 2, the thermo-flow fields

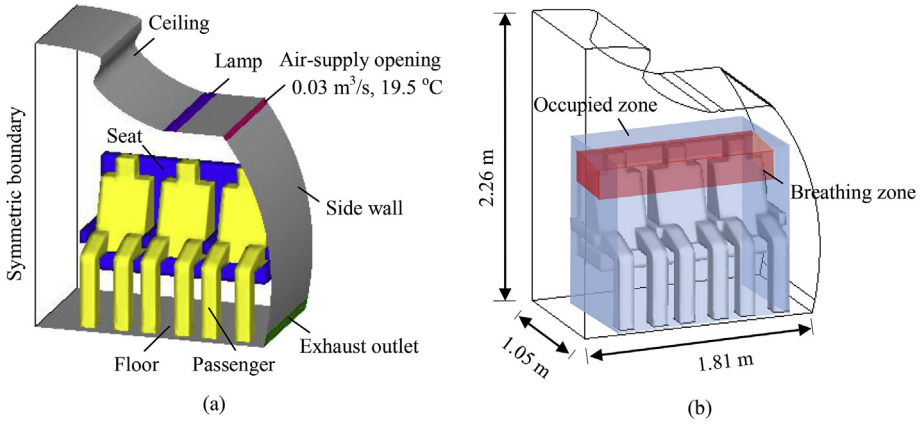

Fig. 3. Half section of a single-aisle aircraft cabin used for an inverse design of the air-supply opening size: (a) cabin geometric model; (b) occupied and breathing zones in which the cabin air environmental performances are evaluated.

were solved for the air-supply opening sizes at the lower and upper bounds, i.e., 0.5 cm and 4.5 cm, respectively. Fig. 4 shows the field distribution in terms of velocity vector, temperature and mean age of air using the full CFD simulation. The flow pattern at different opening sizes is similar. However, with a larger size and thus a smaller air-supply speed, the flow motion is significantly weaker. Flow vortexes are formed near the window with downward flow. The cabin temperature difference between the different opening sizes is not significant, because the air ventilation rate and the supply temperature are the same. The slightly higher air temperature in Fig. 4(c) is due to the fixed wall surface temperatures regardless of the air-supply speeds. The mean age of air is relatively larger near the window for an opening size of 4.5 cm.

To determine the appropriate data samples for the POD analysis, the proposed trial and data sample increase scheme is applied. Fig. 5 depicts the average relative errors and maximum relative errors between the linearly interpolated fields and the fields using the full CFD simulation in the concerned zones. All of the average relative errors for temperature and mean age of air fields are smaller than the set threshold of 10%, as indicated in Fig. 5(c) and (e), so only the average relative errors for the velocity determine the number of adequate data samples. For the first evaluation, the data fields for an opening size of 0.9 cm (S3, 3.929 m/s) are linearly interpolated because its air-supply speed is in the middle of the two original data samples, S1 (0.5 cm, 7.072 m/s) and S2 (4.5 cm, 0.786 m/s). Here, the air-supply speeds instead of the air-supply opening sizes were adopted to evaluate the middle point of the two neighboring data samples. As presented in Fig. 5(a), the average relative error between the linearly interpolated velocity field and the full CFD simulation velocity field for S3 is 16.0%, which is larger than the set threshold 10%, so S3′ should be supplemented into the original two samples.

The second evaluation occurs at S4 (0.65 cm, 5.440 m/s), which is the mid-point of S1 and S3 with reference to the air-supply speed. The third evaluation is at S5 (1.5 cm, 2.357 m/s), which is the mid-point of S2 and S3. Compared with the velocity field using the full CFD simulation, the average relative error of S4 is smaller than the set threshold of 10%. This illustrates that the two CFD samples S1 and S3′ are sufficient for the opening size ranging from 0.5 cm to 0.9 cm. Unfortunately, S5 (1.5 cm, 2.357 m/s) surpasses the set threshold relative error, and S5′ is supplemented into the data samples until S6 (1.1 cm, 3.215 m/s), which is the mid-point of S3′ and S5′, is below the threshold value. Using a similar procedure, S7′ (2.2 cm, 1.607 m/s) and S9′ (3.0 cm, 1.179 m/s) are also supplemented into the data samples until the average relative errors for their neighboring mid-points S8 (1.8 cm, 1.965 m/s), S10 (2.6 cm, 1.360 m/s) and S11 (3.6 cm, 0.982 m/s) are below 10%. Moreover, all of the maximum relative errors at S4, S6, S8, S10 and S11 are smaller than 60%, as shown in Fig. (b), (d) and (f), which illustrates that the nonlinearity among data samples does not substantially prevail. Hence, the six original data samples, S1, S2, S3′, S5′, S7′ and S9′, are sufficient for the POD analysis and should be able to guarantee accuracy due to lack of severe nonlinearity.

4.2. POD analysis for original data samples

Fig. 6(a) presents the respective contribution of each eigenvalue to the general energy when conducting the POD analysis on the six original data samples provided by the full CFD simulation. One eigenvalue corresponds to one eigenvector. It can be seen that the first eigenvector contains nearly all of the energy. The captured energy by each eigenvector decreases drastically from the first to the second and to the third. This may be attributed to the fact that the first one or two eigenvectors substantially contain the basic features of the data samples. Furthermore, Fig. 6(b) depicts the cumulative contribution of the eigenvalues. To capture more than 99.99% of the total energy, the first five eigenvalues (or the first five eigenvectors) are sufficient for the velocity, temperature, and mean age of air.

Fig. 7 presents a comparison of the coefficients of POD modes provided by data interpolation and by CFD. Even by data interpolation, the coefficients for the six original data samples, i.e., air-supply opening sizes of 4.5 cm (0.786 m/s), 3.0 cm (1.179 m/s), 2.2 cm (1.607 m/s), 1.5 cm (2.357 m/s), 0.9 cm (3.929 m/s) and 0.5 cm (7.072 m/s), are obtained using Eq. (8), then the coefficient curves are obtained by shape-preserving interpolation. While all the so-called coefficients by CFD are provided by Eq. (8) for 46 CFD-simulated cases. It can be seen that the interpolation has provided coefficients that are in generally good agreement with those by CFD. The coefficient c_1 for the first POD mode always has the largest amplitude whereas the later modes have smaller amplitudes, which implies that the first several POD modes primarily contribute to the data construction.

Fig. 8 presents the average relative errors defined by Eq. (9) and the maximum relative errors defined by Eq. (10) between the POD constructed fields and the fully CFD simulated fields for 46 different air-supply opening sizes. The reconstruction errors at the six original data samples (0.5 cm, 0.9 cm, 1.5 cm, 2.2 cm, 3.0 cm and 4.5 cm) are almost zero; for the remaining air opening sizes, the errors are relatively large. The larger errors for the remaining opening sizes are caused by both the representativeness of the extracted POD modes and the coefficient interpolation. Nevertheless, all of the relative errors from data construction are smaller than 10% and the maximum relative errors are less than 60%, which indicates that the utilized POD method can provide data fields in good agreement with the full CFD simulation.

4.3. Inversely designed air-supply opening sizes

Based on the constructed field data using the POD, the cabin environmental performance can be rapidly provided. Fig. 9 compares the computed cabin environmental performance versus the air-supply opening sizes between the proposed POD method (black lines with dots) and the full CFD simulation (red dots). Generally, the predicted largest PD and the volumetric-averaged absolute value of the PMV (or |PMV|) in the occupied zone using the POD method agree well with those provided by the full CFD simulation, as shown in Fig. 9(a) and (b), respectively. However, there are a few deviations in the predicted largest mean age of air between both methods as shown in Fig. 9(d). Nevertheless, these deviations are not quite significant for preventing the POD method to be applied in engineering practices.

By increasing the air-supply opening size, the air-supply speed decreases due to the fixed airflow rate. As shown in Fig. 9(a), the draught risk indicated by the PD is thus reduced with the opening size. The volumetric-averaged absolute value of the PMV in the occupied zone initially increases and then slightly decreases, as shown in Fig. 9(b). This is due to the slightly decreasing cabin temperature at a lower air-supply speed because of fixed surface temperature boundary conditions, as shown in Fig. 4(d), causing the |PMV| to slightly decrease when the air-supply opening size is greater than 2.1 cm. Fig. 9(c) shows the |PMV| for an assumed constant surrounding air temperature of 23.5 °C in the cabin-occupied zone. It can be seen that the |PMV| steadily increases when the air-supply opening size increases from 0.5 cm to 4.5 cm. With an increase in the air-supply opening size, the largest mean age of air initially increases, then decreases and again increases, as illustrated in Fig. 9(d). With a decrease in the air-supply speed, the air circulation is worsened, which results in an increase in the largest mean age of air. However, once the air-supply opening size

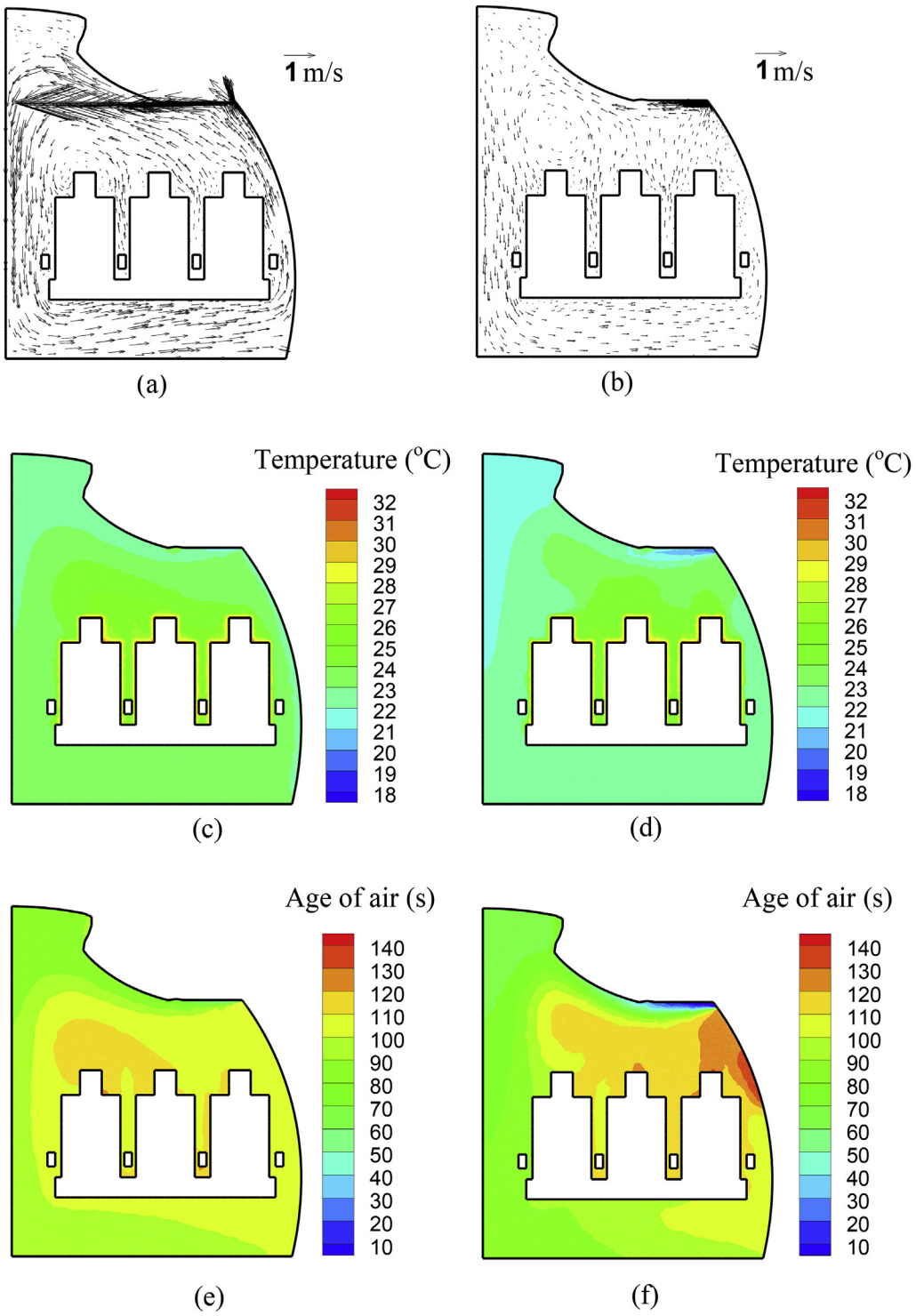

Fig. 4. Thermo-flow field distribution in one section across the aircraft cabin: (a) flow field for an opening size of 0.5 cm; (b) flow field for an opening size of 4.5 cm; (c) temperature field for an opening size of 0.5 cm; (d) temperature field for an opening size of 4.5 cm; (e) mean age of air field for an opening size of 0.5 cm; (f) mean age of air field for an opening size of 4.5 cm.

is greater than 2.1 cm, for which vortexes are generated near the window region at a lower air-supply speed, the largest mean age of air varies with the air-supply opening size in a complex manner.

According to the set criteria of cabin environmental performance, the proper air-supply opening sizes can be determined. Fig. 9(a) shows that if the largest PD in the occupied zone is limited to 25%, then both the POD method and the full CFD simulation specify that the air-supply opening size must be greater than 0.7 cm. Fig. 9(b) illustrates that the air-supply opening size should be less than 1.7 cm when using the CFD simulation and less than 1.8 cm when using the POD method, if the volumetric-averaged absolute value of the PMV in the occupied zone is limited to 0.56. Similarly, the size should be less than 1.2 cm to ensure that the largest mean age of air does not exceed 130 s using the POD

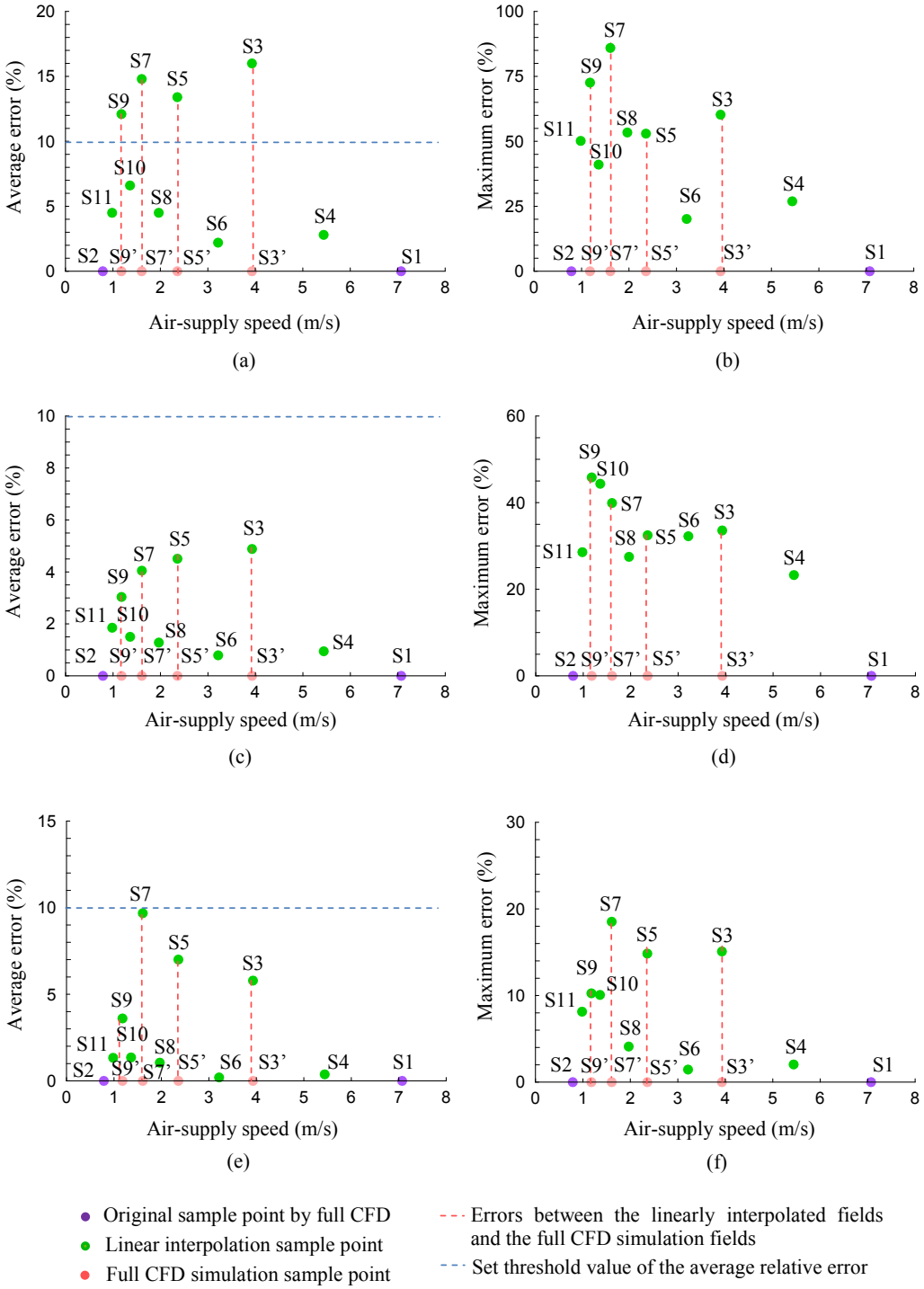

Fig. 5. Relative errors between the linearly interpolated fields and the fields using the full CFD simulation: (a) average relative errors of velocity in the occupied zone; (b) maximum relative errors of velocity in the occupied zone; (c) average relative errors of temperature in the occupied zone; (d) maximum relative errors of temperature in the occupied zone; (e) average relative errors of mean age of air in the breathing zone; (f) maximum relative errors of mean age of air in the breathing zone.

method; a value less than 1.3 cm was provided by the full CFD simulation. Therefore, the air-supply opening size that satisfies these three criteria ranges from 0.7 cm to 1.2 cm using the POD method and 0.7 cm–1.3 cm using the full CFD simulation. This again shows a good accuracy of the proposed POD design method.

5. Discussion

The key factors affecting the accuracy of the POD method are the representativeness of the spatial modes and the accuracy of the coefficients of the spatial modes. Because the spatial modes are extracted from the provided original data samples, the

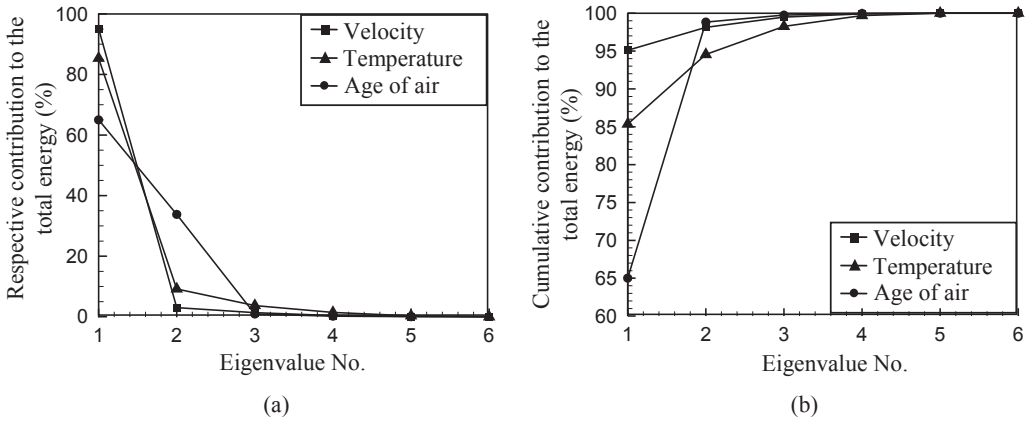

Fig. 6. Contribution of the eigenvalues to the general energy: (a) respective contribution; (b) cumulative contribution.

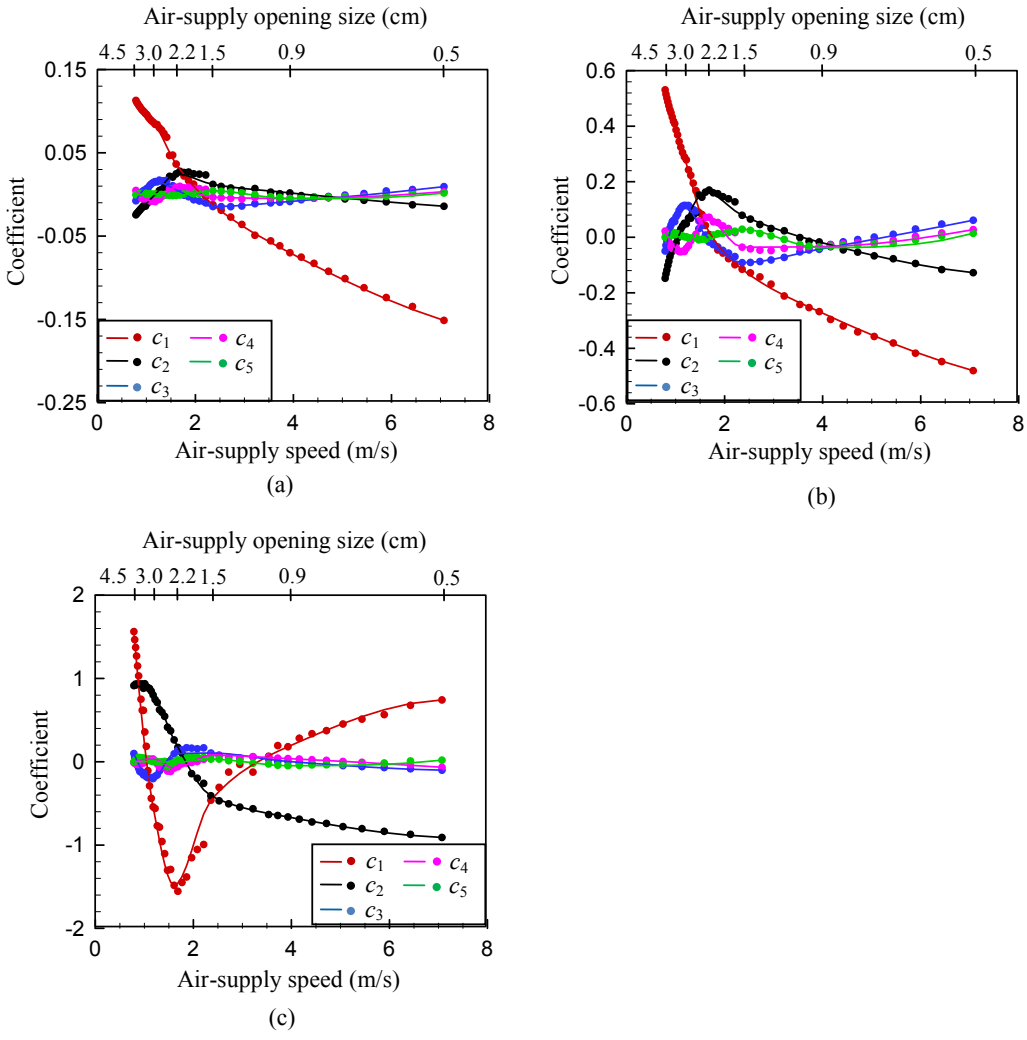

Fig. 7. Coefficients of the spatial modes versus different air-supply speeds for 46 air-supply opening sizes, where curves were provided by data interpolation and points by full CFD simulations: (a) velocity; (b) temperature; (c) mean age of air.

representativeness of the original snapshot data samples is critical. Additionally, the strategies to interpolate the coefficients of the spatial modes are important because different strategies assume different varying trends between the two snapshot data samples. An ideal interpolation uses a minimum number of snapshots but can still provide an excellent approximation of the data.

A trial and data sample increase scheme was proposed in this study. To determine whether the original data samples provided by

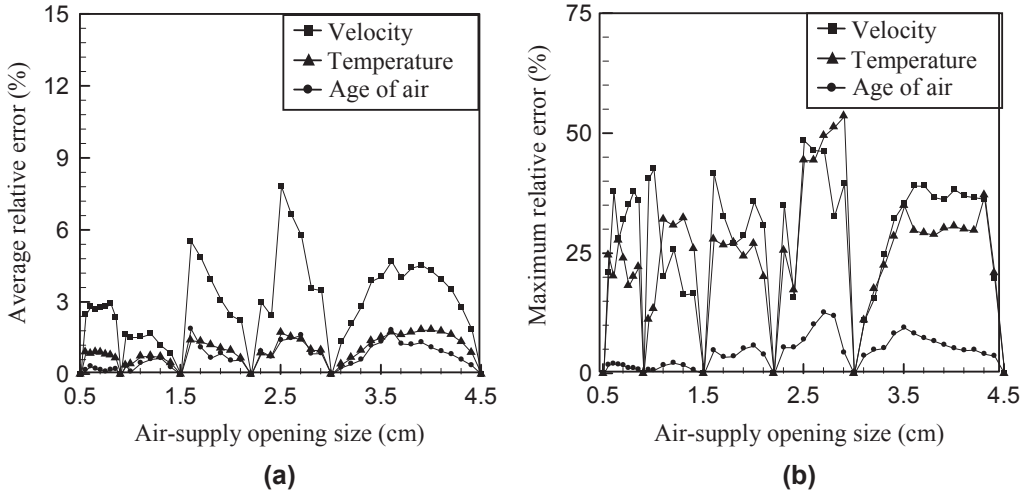

Fig. 8. Relative errors between the POD constructed fields and the fully CFD simulated fields for the velocity and temperature in the occupied zone and the mean age of air in the breathing zone for 46 different air-supply opening sizes: (a) average relative errors; (b) maximum relative errors.

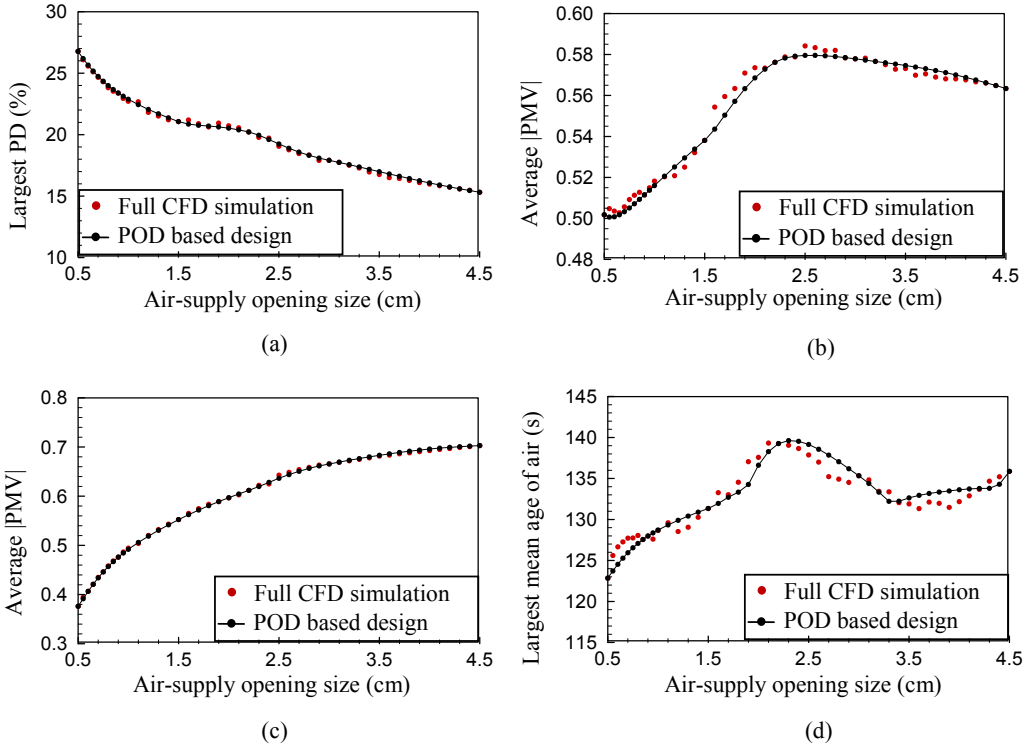

Fig. 9. Comparison of computed cabin environmental performance between the POD method and the full CFD simulation: (a) largest PD in the occupied zone; (b) volumetric-averaged absolute value of PMV in the occupied zone; (c) volumetric-averaged |PMV| in the occupied zone when adopting a constant surrounding air temperature of 23.5 °C; (d) largest mean age of air in the breathing zone.

the full CFD simulation are sufficient, the gaps between the linearly interpolated fields and the fields using the full CFD simulation are evaluated in the middle of two neighboring data samples. This is to ensure that there is no severe nonlinear distribution of the evaluated parameters within both data samples. A limitation of the method is the possibility of omitting some characteristic data samples when the errors in the middle of both neighboring air-supply parameters are correctly within the set threshold error but still have large errors elsewhere. Nevertheless, the occurrence possibility is low, and more data samples can be checked for conservative consideration. A further investigation may also utilize optimization approaches to select the appropriate original data samples from the full CFD simulation.

The piecewise cubic Hermite interpolation (shape-preserving interpolation) was applied to obtain coefficients of the spatial modes between two neighboring original data samples. Because the proposed trial and data sample increase scheme has guaranteed no severe nonlinearity between the two original data samples, a smooth interpolation method that preserves the monotonicity and the shape of the samples can meet the requirement. Further research may try a better coordination scheme between the original data sample preparation and the interpolation of the coefficients of the POD modes.

The POD based design handled only a single design parameter in

Table 2
Comparison of computing time between the POD-based design and the full CFD simulation design.

Method	Providing field data	Determining proper opening sizes	Total computing time
POD method	48.5 h	1 h	49.5 h
Full CFD simulation	368 h	1 h	369 h

this investigation. Further research may investigate multi-parameter design, for which the advantages of POD analysis may be better presented.

Table 2 lists a comparison of the computing time between the POD method and the full CFD simulation method. The computation was implemented in a server equipped with two Intel CPUs (four cores per CPU) of 2.3 GHz and a total of 144 GB of memory. It took 48.5 h to solve for the six original data samples and determine whether the CFD-provided data samples were sufficient. Approximately 1 h was required for the POD analysis to construct the field data for the other 40 cases and determine the proper air-supply opening sizes. However, the full CFD simulation method utilized a total of 368 h to obtain the field data of 46 cases, and 1 h was needed to determine the proper opening sizes. The POD-based design method can save a great amount of computing resources without sacrificing much accuracy.

6. Conclusions

This study proposed a POD-based design approach to efficiently determine proper air-supply opening sizes that satisfy the specific design criteria of cabin environmental performance. The model contains an original data preparation module and a POD-based design module. A trial and data sample increase scheme is utilized to determine whether the original data samples provided by the full CFD simulation are sufficient. By testing the above methodology in a three-dimensional aircraft cabin, the following conclusions are drawn:

- The POD analysis of the original data samples and the interpolation of the coefficients of the spatial modes are able to construct the field data with a generally good accuracy compared with those provided by the full CFD simulation. The inversely determined air-supply opening sizes between the POD-based design and the full CFD simulation are quite similar.
- The POD-based design requires a relatively small amount of computing resources. Most of the computing time for the POD method is spent on preparing the original field data by running a full CFD simulation and determining the sufficiency of these data samples, whereas the POD analysis, interpolation of the spatial mode coefficients, and determination of the proper air-supply opening sizes are efficient. Further research may try a better coordination of the original data sample preparation and interpolation of the coefficients of the spatial modes and conduct multi-parameter design.

Acknowledgments

The work was supported by the National Key Basic Research and Development Program of China (the 973 Program, Grant No.: 2012CB720100) and the Distinguished Young Scholar Program of Liaoning Province (Grant No.: LJQ2013004).

References

[1] T. Zhang, Q. Chen, Identification of contaminant sources in enclosed environments by inverse CFD modeling, Indoor Air 17 (3) (2007) 167–177.
[2] T. Zhang, Q. Chen, Identification of contaminant sources in enclosed spaces by a single sensor, Indoor Air 17 (6) (2007) 439–449.
[3] X. Liu, Z. Zhai, Location identification for indoor instantaneous point contaminant source by probability-based inverse Computational Fluid Dynamics modeling, Indoor Air 18 (1) (2008) 2–11.
[4] X. Liu, Z. Zhai, Prompt tracking of indoor airborne contaminant source location with probability-based inverse multi-zone modeling, Build. Environ. 44 (6) (2009) 1135–1143.
[5] T. Zhang, H. Li, S. Wang, Inversely tracking indoor airborne particles to locate their release sources, Atmos. Environ. 55 (2012) 328–338.
[6] T. Zhang, S. Yin, S. Wang, An inverse method based on CFD to quantify the temporal release rate of a continuously released pollutant source, Atmos. Environ. 77 (2013) 62–77.
[7] T. Zhang, H. Zhou, S. Wang, Inverse identification of the release location, temporal rates, and sensor alarming time of an airborne pollutant source, Indoor Air 25 (2015) 415–427.
[8] W. Liu, T. Zhang, Y. Xue, Z. Zhai, J. Wang, Y. Wei, Q. Chen, State-of-the-art methods for inverse design of an enclosed environment, Build. Environ. 91 (2015) 91–100.
[9] Y. Xue, Z. Zhai, Q. Chen, Inverse prediction and optimization of flow control conditions for confined spaces using a CFD-based genetic algorithm, Build. Environ. 64 (2013) 77–84.
[10] Z. Zhai, Y. Xue, Q. Chen, Inverse design methods for indoor ventilation systems using CFD-based multi-objective genetic algorithm, Build. Simul. 7 (6) (2014) 661–669.
[11] T. Zhang, X. You, Applying neural networks to solve the inverse problem of indoor environment, Indoor Built Environ. 23 (8) (2014) 1187–1195.
[12] J.L. Lumley, The structure of inhomogeneous turbulent flows, in: A. Yaglom, Tatarski (Eds.), Atmospheric Turbulence and Radio Wave Propagation, Nauka Press, Moscow, 1967, pp. 166–178.
[13] P. Holmes, J.L. Lumley, G. Berkooz, Turbulence, Coherent Structures, Dynamical Systems and Symmetry, Cambridge University Press, Cambridge, UK, 1996.
[14] H.P. Bakewell, J.L. Lumley, Viscous sublayer and adjacent wall region in turbulent pipe flow, Phys. Fluids 10 (9) (1967) 1880–1889.
[15] S. Herzog, The Large Scale Structure in the Near-wall Region of Turbulent Pipe Flow, Ph. D. Thesis, Cornell University, 1986.
[16] M.N. Glauser, W.K. George, Orthogonal decomposition of the axisymmetric jet mixing layer including azimuthal dependence, in: Proceedings of the First European Turbulence Conference (Advances in Turbulence), 1987, pp. 357–366. Lyon, France.
[17] L. Sirovich, Turbulence and the dynamics of coherent structures: I–III, Q. Appl. Math. 45 (4) (1987) 561–590.
[18] B. Elhadidi, H.E. Khalifa, Application of proper orthogonal decomposition to indoor airflows, ASHRAE Trans. 111 (1) (2005) 625–634.
[19] P. Ding, X. Wu, Y. He, W. Tao, A fast and efficient method for predicting fluid flow and heat transfer problems, J. Heat Transf. 130 (3) (2008) 1–17.
[20] A. Sempey, C. Inard, C. Ghiaus, C. Allery, Fast simulation of temperature distribution in air conditioned rooms by using proper orthogonal decomposition, Build. Environ. 44 (2) (2009) 280–289.
[21] C. Allery, C. Beghein, A. Hamdouni, Applying proper orthogonal decomposition to the computation of particle dispersion in a two-dimensional ventilated cavity, Commun. Nonlinear Sci. Numer. Simul. 10 (8) (2005) 907–920.
[22] K. Li, W. Xue, X. Chao, H. Su, Optimization of ventilation system operation in office environment using POD model reduction and genetic algorithm, Energy Build. 67 (2013) 34–43.
[23] S. Ahuja, E. Cliff, S. Narayanan, Reduced-order modeling for control of indoor building airflows, in: Proceedings of the 5th National Conference of IBPSA-USA, 2012, pp. 1–8. Madison, Wisconsin, USA.
[24] A. Tallet, F. Allard and C. Allery. Numerical simulation of real-time air flow control by POD/ROM applied to anisothermal ventilated cavity. In: Proceedings of the 10th International Conference on Healthy Buildings, pp. 1960–1965, (Brisbane, Queensland, Australia).
[25] K. Li, H. Su, J. Chu, C. Xu, A fast-POD model for simulation and control of indoor thermal environment of buildings, Build. Environ. 60 (2013) 150–157.
[26] T.R. Smith, J. Moehlis, P. Holmes, Low-dimensional modelling of turbulence using the proper orthogonal decomposition: a tutorial, Nonlinear Dyn. 41 (1–3) (2005) 275–307.
[27] T. Zhang, Q. Chen, Novel air distribution systems for commercial aircraft cabins, Build. Environ. 42 (4) (2007) 1675–1684.
[28] ASHRAE, ASHRAE Handbook - Fundamentals, American Society of Heating, Refrigerating and Air-Conditioning Engineers, Atlanta, 2009.
[29] P.O. Fanger, in: E. Robert (Ed.), Thermal Comfort, Krieger Publishing Company, Malabar, FL, 1982.
[30] M. Sandberg, What is ventilation efficiency? Build. Environ. 16 (2) (1981) 123–135.